Brain Structure and Function (2019) 224:1457–1467
https://doi.org/10.1007/s00429-019-01848-2

ORIGINAL ARTICLE

A framework for cortical laminar composition analysis using low-resolution T1 MRI images

Ittai Shamir[1] · Omri Tomer[2] · Zvi Baratz[2] · Galia Tsarfaty[3] · Maya Faraggi[1] · Assaf Horowitz[2] · Yaniv Assaf[1,2]

Received: 16 August 2018 / Accepted: 11 February 2019 / Published online: 19 February 2019

Abstract

The layer composition of the cerebral cortex represents a unique anatomical fingerprint of brain development, function, connectivity, and pathology. Historically, the cortical layers were investigated solely ex-vivo using histological means, but recent magnetic resonance imaging (MRI) studies suggest that T1 relaxation images can be utilized to separate the layers. Despite technological advancements in the field of high-resolution MRI, accurate estimation of whole-brain cortical laminar composition has remained limited due to partial volume effects, leaving some layers far beyond the image resolution. In this study, we offer a simple and accurate method for cortical laminar composition analysis, resolving partial volume effects and cortical curvature heterogeneity. We use a low-resolution 3T MRI echo planar imaging inversion recovery (EPI IR) scan protocol that provides fast acquisition (~ 12 min) and enables extraction of multiple T1 relaxation time components per voxel, which are assigned to types of brain tissue and utilized to extract the subvoxel composition of six T1 layers. While previous investigation of the layers required the estimation of cortical normals or smoothing of layer widths (similar to VBM), here we developed a sphere-based approach to explore the inner mesoscale architecture of the cortex. Our novel algorithm conducts spatial analysis using volumetric sampling of a system of virtual spheres dispersed throughout the entire cortical space. The methodology offers a robust and powerful framework for quantification and visualization of the cortical laminar structure on the cortical surface, providing a basis for quantitative investigation of its role in cognition, physiology and pathology.

Keywords Neuroimaging · Brain mapping · Gray matter · Image processing · Computational biology

Introduction

Study of the laminar structure of the cerebral cortex was first made possible in the beginning of the twentieth century ex-vivo through the use of histological methods (Garey 2006). Years later, renowned neuroanatomist Gerhardt von Bonin famously stated in an article on the cerebral cortex that "the cortex is both chaos and order, and therein lies its strength" (Von Bonin 1950). On the chaos side, the cerebral cortex has a highly tortuous surface consisting of many gyri and sulci with an overall thickness that varies regionally between 2 and 4 mm on average throughout cortical regions. On the order side, the cortex is characterized by a highly organized laminar structure consisting of six cortical layers, each characterized by different types of neurons. While the order of the cortical layers remains constant, the thickness of each layer varies regionally throughout cortical regions and therein lies its "strength". The layers are initially formed during brain development, when neurons migrate to form the cortex, playing an important role in brain connectivity and function. The layers and their composition are assumed to play an integral role in the function, development and pathology of the brain (Kiernan et al. 2014).

With the advent of MRI, visualization of the overall cortical thickness using T1-weighted MRI images has been successfully achieved. Cortical thickness visualization includes accurate delineation of the inner cortical surface, bordering with myelin rich white matter, and the outer cortical surface, bordering with pia matter and the surrounding cerebral spinal fluid (Kiernan et al. 2014; Scholtens et al. 2015). Recent studies suggest that T1

✉ Yaniv Assaf
assafyan@gmail.com

[1] Department of Neurobiology, Faculty of Life Sciences, Tel Aviv University, Ramat Aviv, 69978 Tel Aviv, Israel

[2] Sagol School of Neuroscience, Tel Aviv University, Tel Aviv, Israel

[3] Department of Diagnostic Imaging, Sheba Medical Center, Tel Hashomer, Ramat Gan, Israel

relaxation images can also be utilized to provide layer-specific information, using either high-resolution at high magnetic field or subvoxel modeling at lower resolutions. These approaches use a variety of MRI images, including T1, T2 and T2* weighted images, as well as R1, R2, and R2* susceptibility images (Shafee et al. 2015; Duyn et al. 2007; Barbier et al. 2002; Bridge et al. 2006; Glasser et al. 2014; Deistung et al. 2013; Lutti et al. 2014).

The T1 MRI approach to imaging the substructure of the cortex has shown great potential. An early IR MRI study of both rat and human cortices revealed at least six T1 clusters, demonstrated on the striate cortex (stripe of Gennari) and the frontal cortex. Since it has been established that myelination causes shortening of T1, each cluster will decrease in T1 values from the outermost to the innermost parts of the cortex (Clark et al. 1992). Comparison with histology of rat brains revealed a correspondence between the cortical layers and the T1 clusters, although these two measures represent different quantities (Barazany and Assaf 2012).

A larger scale follow-up study of entire rat and human cortices used the same IR MRI protocol as well as a higher resolution version of the protocol. The study revealed that the six clustered T1 components along the cortex have similar values throughout subjects, and concluded that low-resolution multi-T1 mapping, combined with composition analysis, could provide practical means for measuring the T1 layers (Lifshits et al. 2018). Still, whole-brain automatic analysis and visualization of the cortical substructure remains one of the most significant neuroimaging challenges of recent years.

Visualization of the cortical laminar components remains hindered by two main imaging challenges. The first challenge involves partial volume effect (PVE), an imaging effect occurring when voxel size exceeds the size of tissue detail (Ballester et al. 2002). Our premise is that the solution to imaging the cortical layers does not necessarily lie in increasing T1 MRI resolution, since even such high-resolution images are afflicted by PVE, posing a limiting factor in visualization of the cortical laminar structure (Lifshits et al. 2018). The second challenge involves the intricate geometry of the cortex, which has been typically approached either by estimating normals to the cortical surfaces and investigating the layer composition along them, or by smoothing layer widths, similar to voxel-based morphometry (VBM) (Barazany and Assaf 2012; Annese et al. 2004; Waehnert et al. 2014). The applicability of such approaches is limited, not only because minor errors in cortical surface estimation can lead to greater errors in normal estimations, but also because this process has to be repeated accurately throughout the entire cortex.

In this work, we present a method for investigating the laminar substructure of the cortex through subvoxel modeling at lower resolution T1 MRI. We use a low-resolution echo planar imaging inversion recovery (EPI IR) protocol that provides fast acquisition (~ 12 min) and enables extraction of multiple T1 components per voxel, which are assigned to brain tissue types and utilized to extract the subvoxel composition of each T1 layer (Lifshits et al. 2018; Barazany and Assaf 2012; Peel et al. 2000; Tomer et al. 2018). We then explore the mesoscale laminar architecture of the cortex using a sphere-based approach, implementing a geometric solution based on cortical volume sampling using a system of virtual spheres dispersed throughout the entire cortex. A spherical shape was chosen due to its symmetry and invariance to rotation, offering a simple and robust alternative to cortical normals.

Our methodology offers an automated and unbiased whole-brain solution to investigating the complex mesoscale laminar architecture of the cortex. We suggest that our powerful tool for investigating the cortical laminar structure could enable expansion of studies on the role of cortical thickness in brain function and behavior to the cortical layer level.

Materials and methods

Subjects

Fifteen healthy human subjects were recruited for this study ($N = 15$), including 7 male and 8 female, 23–43 years, all right handed. Subjects were neurologically and radiologically healthy, with no history of neurological diseases, and normal appearance of clinical MRI protocol. The imaging protocol was approved by the institutional review boards of Sheba Medical Centers and Tel Aviv University, where the MRI investigations were performed. All subjects provided signed informed consent before enrollment in the study.

MRI acquisition

All experiments were scanned on a 3T Magnetom Siemens Prisma (Siemens, Erlangen, Germany) scanner with a 64-channel RF coil.

Two T1-weighted MRI sequences were used to characterize the cortical layers:

1. An inversion recovery echo planar imaging (IR EPI) sequence, with the following parameters: TR/TE = 10,000/30 ms and 60 inversion times spread between 50 ms up to 3,000 ms, voxel size $3 \times 3 \times 3$ mm^3, image size $68 \times 68 \times 42$ voxels, each voxel fitted with up to 7 T1 values (Lifshits et al. 2018) (see below). The acquisition time for the inversion recovery data set was approximately 12 min.

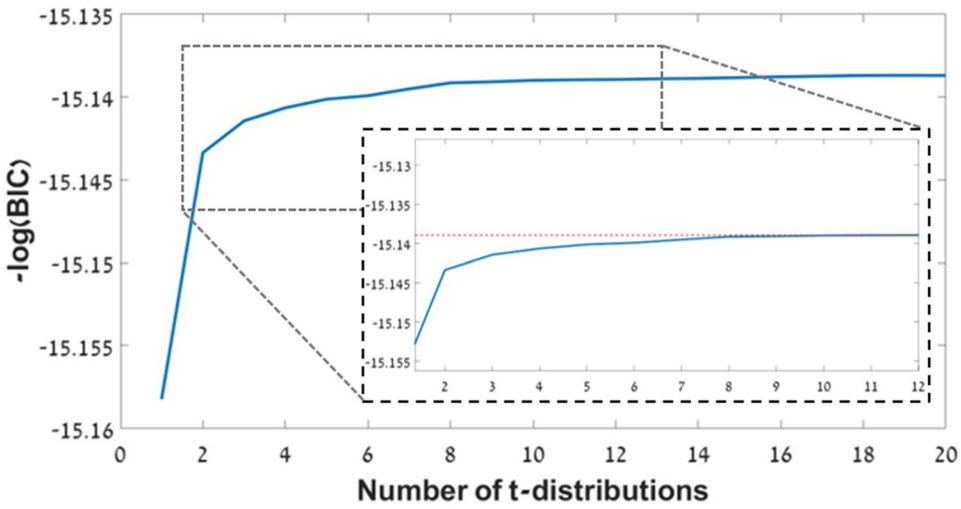

Fig. 1 Evaluation of mixture of t-distributions fit. For all 15 subjects, the mixture was repeatedly fit to the T1 histogram, using a varying number of distributions, ranging between 1 and 20 distributions. −Log of the average Bayesian Information Criterion (BIC) for all subjects was evaluated for each instance, revealing a maximal value at around 11 distributions (red line), followed by a plateau at larger numbers of distributions

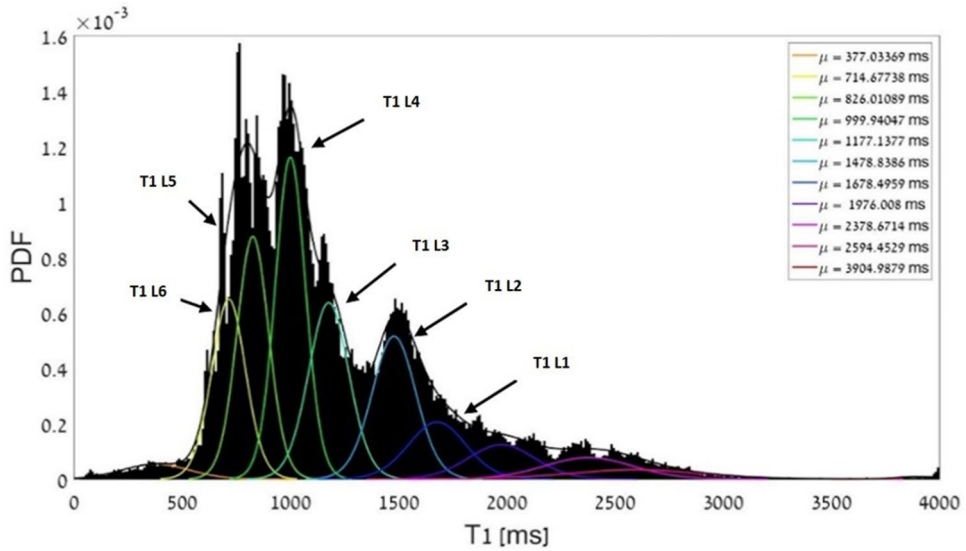

Fig. 2 T1 histogram (black bins) fit to a mixture of t-distributions (black outline). The mixture is made up of 11 individual t-distributions (color map). Each μ_k represents an expected value of a single t-distribution, or center of its curve. It is worth noting again that T1 is not considered a direct measure of cytoarchitecture, but rather a measure of myelination (Clark et al. 1992). T1 layers with higher indices (or smaller T1 values) are more myelinated and are, therefore, located deeper in the cortical cross section. For this reason, t-distributions 2, 3, 4, 5, 6, and 7 are termed T1 layers 6, 5, 4, 3, 2, and 1, respectively

2. An MPRAGE sequence, with the following parameters: TR/TE = 1750/2.6 ms, TI = 900 ms, voxel size 1 × 1 × 1 mm^3, image size 224 × 224 × 160 voxels, each voxel fitted with a single T1 value. This sequence was used as an anatomical reference with high gray/white matter contrast.

IR decay function fit

The IR EPI data were used for multiple T1 analysis, by calculating T1 values and their corresponding partial volumes on a voxel-by-voxel basis. The IR data sets were fitted to the conventional inversion recovery decay function with up to 7 possible T1 components per voxel (Lifshits et al. 2018):

$$M(TI_i) = \sum_{j=1}^{7} M0_j \cdot \left(1 - 2e^{-\frac{TI_i}{T_{1j}}}\right), \quad (1)$$

where $M(TI_i)$ magnetization at the ith inversion recovery image; in other words ,the magnetization measured for each specific T1 component. $M0_j$ predicted magnetization at TI = 0 ms for each T1 component (j) in the voxel. T_{1j} longitudinal relaxation time for each T1 component. j was set

up to 7 for the low-resolution experiments, indicating fit to seven individual exponential fits, based on the assumption that there are 7 T1 components in the tissue—1 for CSF, 1 for WM and heavily myelinated layer of the cortex and additional 5 cortical layers.

Normalization of each of the predicted magnetization values according to $\frac{M0_j}{\sum_{i=1}^{j} M0_j}$ then represents the voxel contribution of each corresponding T1 component (j).

T1 probabilistic classification

The multiple T1 components were used for accurate whole-brain classification to brain tissues on a voxel-by-voxel basis. A T1 histogram was initially plotted for this purpose. Each IR EPI set of images consists of up to ~ 1.36×10^6 potential T1 values: $68 \times 68 \times 42$ [voxels] $\times 7$ [T1 fitted values]. To represent all fitted T1 values according to their partial volumes in the histogram, each voxel was given a weight greater than one.

The T1 histogram was then fitted to a probabilistic mixture model (similar to the method shown in Lifshits et al. 2018; Barazany et al. 2012), consisting of t-distributions (Peel et al. 2000; Tomer et al. 2018). The probability of each t-distribution in the voxel was calculated using Bayes' formula:

$$P_k = \sum_{i=1}^{7} f_i \cdot \frac{p\left(T_{1(i)}|k\right)p(k)}{p\left(T_{1(i)}\right)}, \tag{2}$$

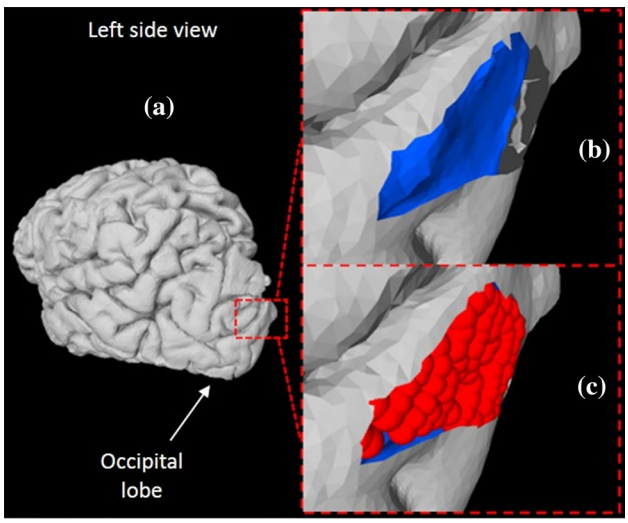

Fig. 3 Cortical volume sampling: left side view of the occipital lobe of left hemisphere, where the outer cortical surface is represented in gray (**a**), the underlying inner cortical surface is represented in blue (**b**) and the cortical volume sampled between the two is represented by red spheres (**c**)

where k is a specific t-distribution. $T_{1(i)}$ is the T1 value of the ith component of the voxel. f_i is the partial volume of $T_{1(i)}$ (normalized as shown in the previous section). $p\left(T_1\right)$ is the general whole-brain probability of a T_1 value. $p(k)$ is the probability of t-distribution k. $p\left(T_1|k\right)$ is the probability of the T_1 value in t-distribution k.

This model was used as a means of probabilistic classification of T1 values per subject into clusters. Selection of the appropriate number of t-distributions for the mixture model was completed using the Bayesian information criterion (BIC), a criterion used for probabilistic model selection. BIC uses a log likelihood function and penalizes for more complex models with additional parameters. The mixture model was fitted repeatedly using a different number of distributions each time, ranging between 1 and 20 distributions, and evaluated using −log of BIC value (see Fig. 1).

Fit to 11 t-distributions was deemed sufficient, where −log(BIC) reaches a maximal value with the fewest distributions. These 11 distinct T1 clusters correspond to different types of brain tissue (see Fig. 2):

1. White matter (WM) characterized by low T1 values, represented by 1st t-distribution.
2. Gray matter (GM) characterized by mid-range T1 values, represented by 2nd–7th t-distributions corresponding to 6 T1 layers, with decreasing degrees of myelination. Because of the link between myelination and shorter T1 values, T1 layer 6 (2nd t-distribution) represents the most highly myelinated and innermost cortical component, with decreasing degrees of myelination moving outwards up to the outermost cortical component—T1 layer 1 (7th t-distribution).
3. Cerebral spinal fluid (CSF) characterized by high T1 values, represented by 8th–11th t-distributions.

It is worth noting that while the T1 clusters representing CSF and WM exhibited high inter-subject variability, mainly due to signal noise, those representing gray matter exhibited very low inter-subject variability. This finding suggests a robustness regarding modeling the laminar structure of the cortex.

Image registration

In the interest of accurately sampling T1 layer probability maps inside the cortical spheres, all T1 layer probability maps were registered to the anatomical MPRAGE image. Registration was completed in SPM12 using a rigid body transformation with the first IR image (IR1) as the source image.

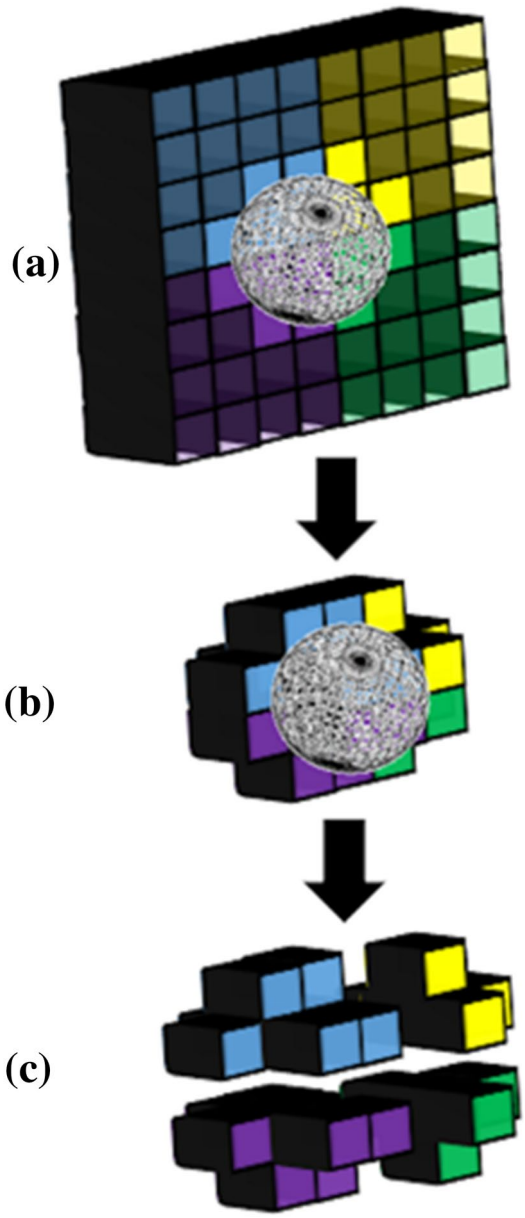

Fig. 4 Schematic representation of voxel partitioning. A sphere is located between several voxels, in this case 4 voxels: blue, yellow, green and purple (**a**). Each voxel is divided into subvoxels, 4^3 subvoxels in this case, leaving only those contributing to the volume of the sphere (**b**). The sphere's weights are assigned according to each voxel's contributing portion of subvoxels to its volume (**c**)

Cortical volume sampling

To provide accurate volumetric sampling of the complex geometry of the cortex, we offer a simple geometric alternative to cortical normals by creating a sampling system of virtual spheres filling the entire cortex volume. A spherical shape was chosen as due to its symmetry and invariance to rotation, minimizing errors in cortical normals associated with surface calculations and consequently enabling more accurate sampling and localization throughout the cortex. The following steps were taken to create and implement this volumetric sampling system:

1. Cortical surface delineation: The anatomical MPRAGE image was analyzed and segmented in the *FreeSurfer* pipeline (Fischl 2012), delineating the following three cortical triangular surfaces:
   a. Inner surface—cortical GM bordering with the underlying WM.
   b. Mid surface—an estimation of the center of cortical GM, based on the inner and outer surfaces.
   c. Outer surface—cortical GM bordering with the surrounding CSF.
2. Sampling system generation: The cortical surfaces were then used a frame for building our sampling system. Each such cortical surface is represented by a triangular mesh, consisting of vertices—corresponding to points in space (~ 150,000 per hemisphere) and faces—corresponding to three vertices per triangle. Each sphere was centered on a vertex on the mid surface, with its top tangential to the outer surface and its bottom tangential to the inner surface. Since the resulting average sphere radius is ~ 1 mm and the average distance between adjacent vertices on the surface is ~ 1 mm, volumetric overlap between spheres occurs. To sample the entire cortex and yet avoid excessive volumetric overlap, sampling rate was improved by subsampling the mid surface vertices by a factor of 2 to ~ 75,000 spheres per hemisphere (see Fig. 3).
3. Data sampling: One of the main challenges in implementing spherical sampling of low-resolution data lies in the resolution difference between the spherical sampling system (average radius of ~ 1 mm) and the T1 data ($3^3 mm^3$). Overcoming this resolution gap demanded a super-resolution solution based on estimation of subvoxel information. Our offered solution includes the following steps:
   a. Partitioning each voxel into subvoxels: Degree of partitioning was chosen so that each subvoxel has the largest volume while still enabling accurate group representation of a spherical volume with a radius of 1 mm. Consequently, each voxel was partitioned into 10^3 subvoxels, each assigned location properties, primarily its location inside or outside of a given sphere.
   b. Assignment of spherical volume weights: Each sphere in our sampling system was assigned weights, corresponding to each voxel's contribution

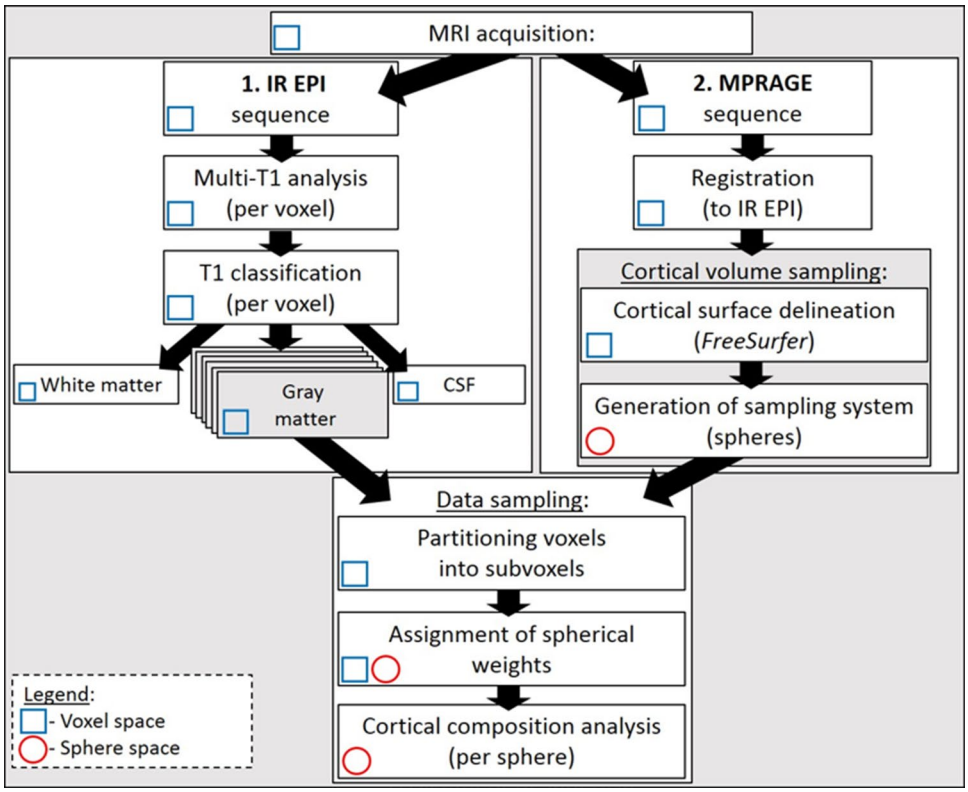

Fig. 5 Streamline summary of our framework for cortical layer composition analysis, from MRI acquisition to data sampling

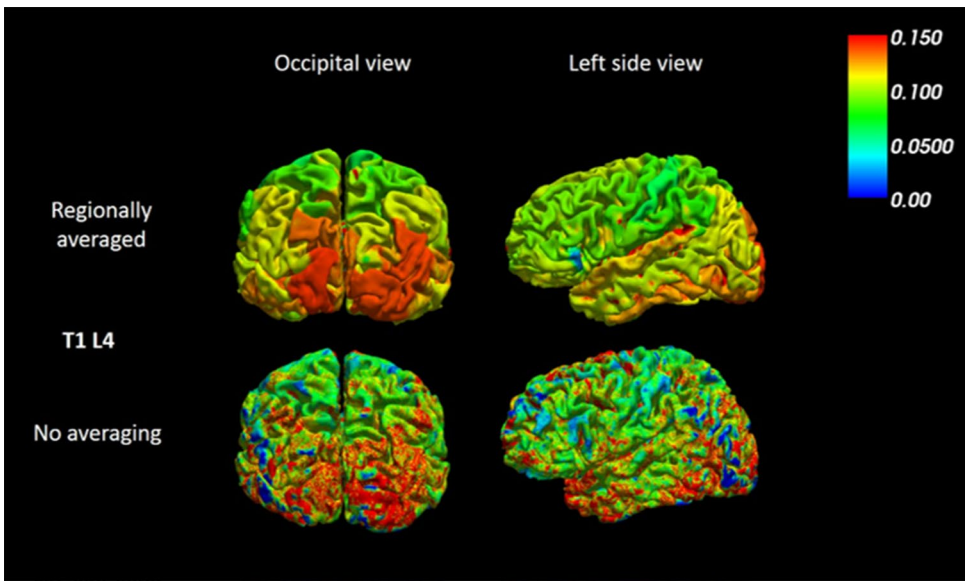

Fig. 6 Single subject's T1 layer 4 probability maps, with averaging to 75 regions according to Destrieux atlas (top row), and without any averaging (bottom row). Regional averaging was completed not only as a smoothing method to better visualize the T1 layer probability maps, but also to overcome intra-regional variability caused by thickness and laminar content variations between sulci and gyri (as seen in the bottom row)

to its spherical volume (see Fig. 4), according to the following equation:

$$W_{\text{voxel}_i,\text{sphere}_j} = \frac{N_{\text{voxel}_i,\text{sphere}_j}}{N_{\text{sphere}_j}}, \quad (3)$$

where $W_{\text{voxel}_i,\text{sphere}_j}$ is the volume weight of voxel i per sphere j. $N_{\text{voxel}_i,\text{sphere}_j}$ is the number of subvoxels from voxel i located inside sphere j. N_{sphere_j} is the total number of subvoxels located inside sphere j.

c. Cortical composition analysis inside sphere: to estimate the cortical composition inside our sampling sys-

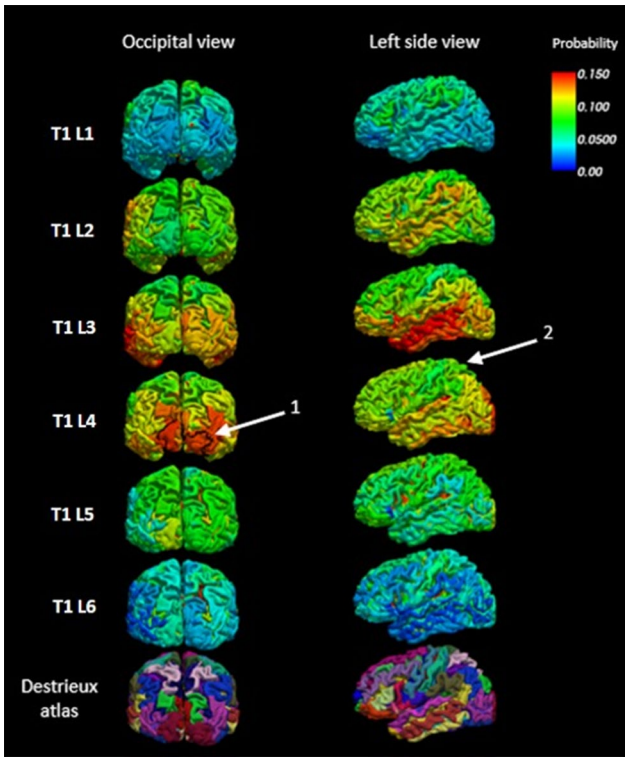

Fig. 7 Single subject T1 layer probability maps (T1 L1–T1 L6), averaged per each of the 75 regions in Destrieux Atlas. Arrows indicate interesting features: arrow 1 indicates high T1 layer 4 presence in the primary visual area (V1 outlined in black), and arrow 2 indicates lower presence in the motor cortex

tem, each sphere's volume weight was multiplied by their corresponding voxel's entire probabilistic content (see T1 probabilistic classification). In other words, the assignment of spherical weights does not make any assumptions regarding layer order. The process was repeated across all spheres in our entire sampling system, according to the following equation:

$$\mathrm{P}\left(\frac{t_k}{\mathrm{sphere}}\right) = \sum_{i=1}^{M}\sum_{k=2}^{7} W_{\mathrm{voxel}_i,\mathrm{sphere}_j} \cdot \mathrm{P}\left(\frac{t_k}{\mathrm{voxel}_i}\right), \qquad (4)$$

where $\mathrm{P}(t_k/\mathrm{sphere})$ is the probability of t-distribution k per sphere. k-t-distributions 2, 3,..., 7, representing T1 layers 6, 5,..., 1, respectively. M is the number of voxels within which sphere j lies. $W_{\mathrm{voxel}_i,\mathrm{sphere}_j}$ is the volume weight of voxel i per sphere j. $\mathrm{P}(t_k/\mathrm{voxel_i})$ is the probability of t-distribution k in voxel i.

The entire streamline was repeated for each of the 15 subjects (for an overview of the entire streamline, see Fig. 5).

Results and discussion

Use of the cortical spheres enabled a rotationally invariant estimation of layer composition within the cortex with simple projection of the quantitative layer width onto the surface. In other words, implementation of our methodology resulted in six multidimensional data sets per subject, each consisting of ~ 150,000 spheres dispersed throughout both hemispheres and revealing individual T1 layer compositions.

The results were visualized by projecting each T1 layer composition onto the subject's cortical mid surface. Because of a high variability in thickness and laminar structure between gyral caps and sulcal fundi (MacDonald et al. 2000), cortical sphere laminar compositions were averaged regionally (see Fig. 6). In other words, to better conduct exploratory spatial analysis of each layer composition, intra-subject values were averaged regionally throughout 75 different cortical regions, using FreeSurfer's automatic surface-based parcellation atlas Destrieux (Fischl et al. 2004) (see Fig. 7).

The process was repeated for 15 subjects, and then, inter-subject cortical composition values were averaged again per each of the 75 Destrieux atlas regions. Results were visualized by projecting each averaged layer composition onto a cortical surface representing the average brain of all 15 subjects (see Fig. 8).

Visual assessment of these surface projections reveals that the innermost and the outermost layers, corresponding to T1 layers 1 and 6, exhibit the lowest compositional values in comparison with T1 layers 2, 3, 4, and 5. More specifically, an interesting feature recurring across subjects is the high intensity of T1 layer 4 in the primary visual area (V1), accompanied by low intensity in the motor cortex.

Quantitative assessment of the T1 layer compositions was conducted by registering all 15 subjects and the average brain to a FreeSurfer mapping of the Von Economo—Koskinas atlas (Scholtens et al. 2016), which represents a cytoarchitectonic division of the cortex into over 40 regions based on histological findings. To select a set of distinctly different cortical regions, a granularity atlas was also used (similar to the process shown in Beul et al. 2014 and in; Scholtens et al. 2015). The granularity atlas classifies these cortical regions into six granularity indices, from the least granular allocortex regions up to the granular cortical regions. Six different cortical regions were chosen and their T1 layer compositions were averaged (see Fig. 9).

Once again, T1 layers 2–5 exhibit a more dominant presence throughout the cortex, compared to layers 1 and 6. T1 layers, which are closer to white matter both physically as well as in cytoarchitecture (T1 layers 3–6), exhibit an increasingly high presence in more granular regions (such as the area striata and the area peristraita), while the outermost

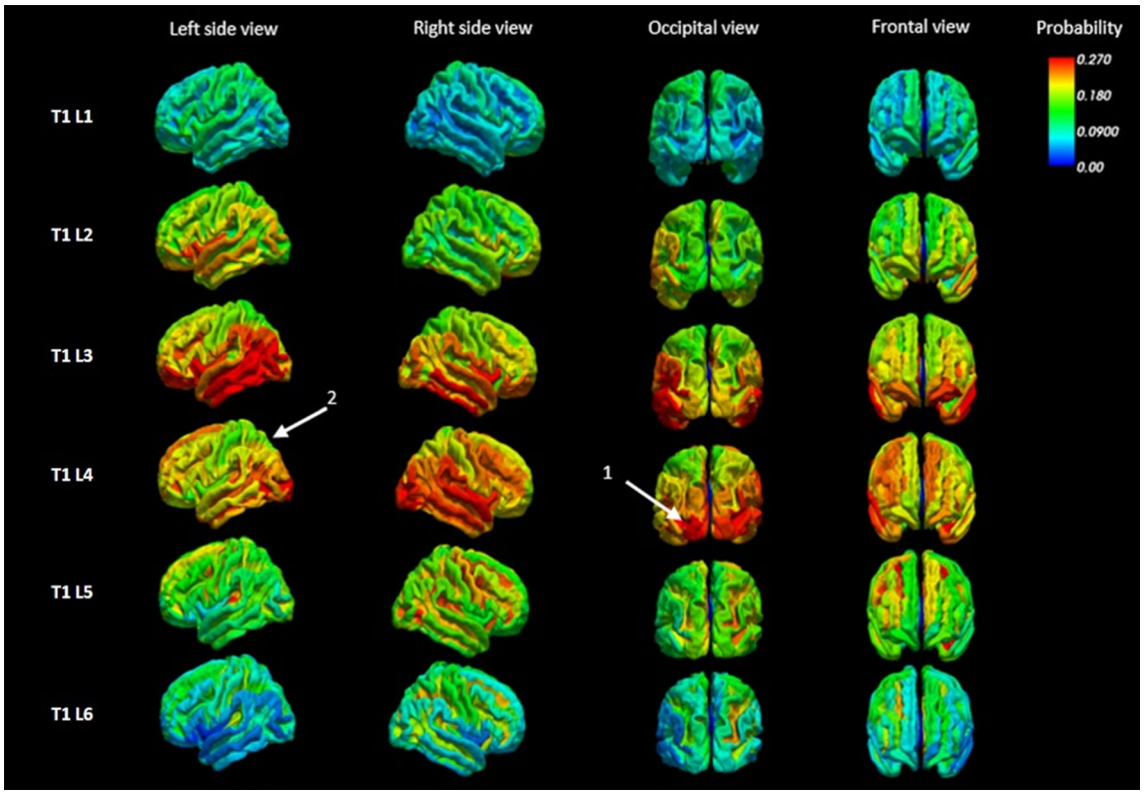

Fig. 8 15 subject average T1 layer probability maps (T1 L1–T1 L6), averaged per each of the 75 regions in Destrieux Atlas. Arrows indicate the recurring interesting features from single subject analysis (see Fig. 4). Arrow 1 indicates high T1 layer 4 presence in the primary visual area and arrow 2 indicates lower presence in the motor cortex

less myelinated T1 layers (layers 1 and 2) exhibit a decreasing presence in such granular regions.

Conclusions

In this work, we propose an automated and unbiased methodology for whole-brain investigation of the complex mesoscale laminar architecture of the cortex. The methodology is based on a surface-wise T1 layer composition analysis of inversion recovery echo planar imaging (IR EPI), which enables extraction of multiple T1 relaxation time components per voxel. The novelty lies in the use of rotationally invariant cortical spheres, sampling the regionally varying cortical thickness across the tortuous cortical folding. The selectivity of T1 measures to the cortex combined with conventional cortical surface estimation, on which our sampling system of spheres is based, overcome the low resolution of the acquired IR MRI and allow representation of layer widths in a 3D in objective manner.

While MRI visualization of the overall cortical thickness has been successfully achieved (Fischl et al. 2010; Scholtens et al. 2015), to this day, there lacks a single automatic whole-brain approach for investigating the laminar structure of the cortex. There are two main opposing approaches for investigating the cortex through the use of T1 MRI. The first approach uses high resolution at high magnetic field, typically at the level of laminar width but on a small volume of the brain (Duyn et al. 2007; Barbier et al. 2002; Lifshits et al. 2018; Geyer et al. 2011; Clare et al. 2005; Turner et al. 2008; Dinse et al. 2015; Fracasso et al. 2016; Waehnert et al. 2016). The second approach uses whole-brain subvoxel modeling at lower resolutions, which creates a localization challenge (Lifshits et al. 2018; Barazany and Assaf 2012). The reason for the limited applicability of the abovementioned approaches is twofold. On one hand is PVE when cortical layer detail exceeds even the resolution of high-resolution images of the cortex (Ballester et al. 2002; Lifshits et al. 2018). PVE is commonly dealt with by smoothing layer widths (similar to VBM), which decreases level of tissue detail (Barazany and Assaf 2012). On the other hand is the localization challenge inside the complex geometry of cortex, which demanded the estimation of cortical normals (Barazany and Assaf 2012; Annese et al. 2004; Waehnert et al. 2014), a semi-subjective process prone to errors due to inaccuracies in surface modeling (Lifshits et al. 2018).

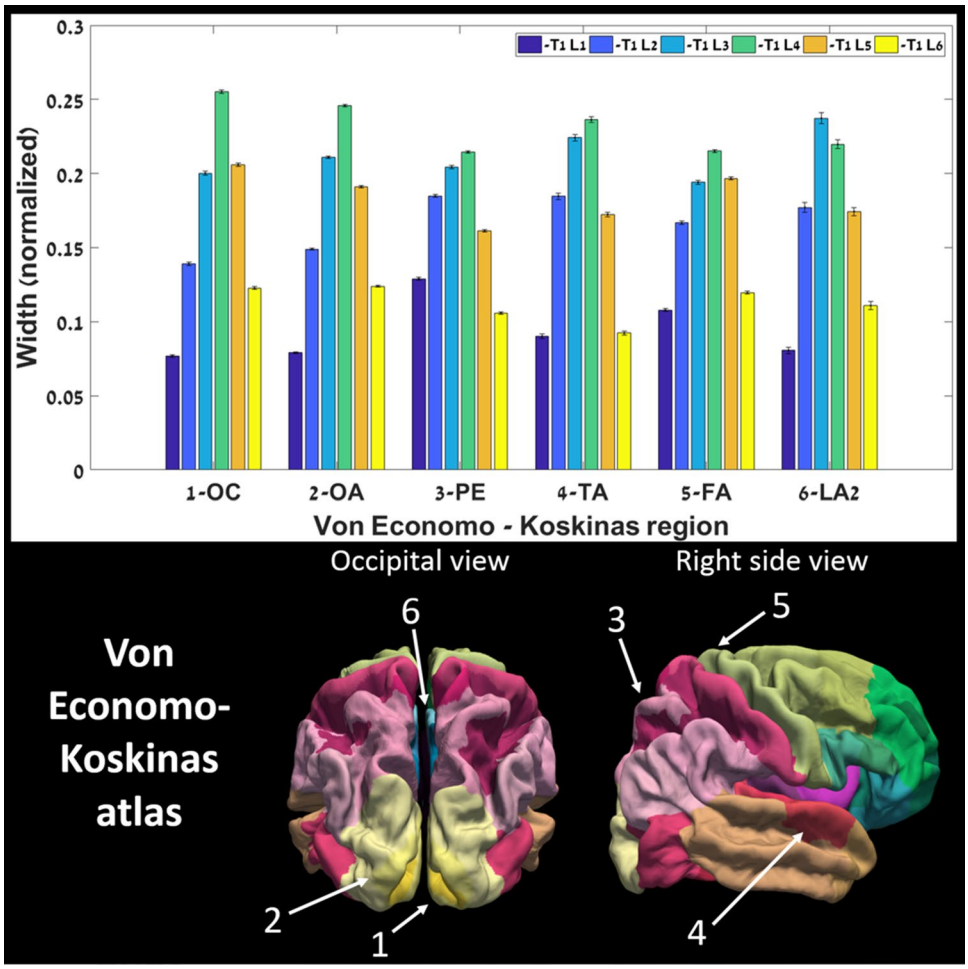

Fig. 9 Distribution of T1 layers across six different cortical regions (top). Results are based on 15 subject average T1 layer probability maps (see Fig. 8), registered to the Von Economo—Koskinas atlas (bottom), where the selected regions represent regions with decreasing granularity indices, as follows: region 1 (OC) is the area striata granulosa, region 2 (OA) is the area peristriata, region 3 (PE) is the area parietalis superior, region 4 (TA) is the area temporalis superior, region 5 (FA) is the area praecentralis, and region 6 (LA2) is the area limbicus anterior agranularis—cingularis anterior

Here, we achieve super-resolution by estimating subvoxel information from a multi-T1 data set inside a sampled system of volumetric cortical spheres. Our method has several main advantages: (1) use of a standard MRI protocol and scanner setup (IR EPI and MPRAGE); (2) quick acquisition of a low-resolution data set (~ 12 min); (3) investigation of the laminar structure of the cortex in an automated whole-brain 3D manner, overcoming both PVE as well as the need for cortical normals; (4) enabling easy visualization of laminar composition through the use of laminar surface projections; and (5) demonstration of transition between various brain regions solely based on laminar composition. Most notably, our method demonstrates accurate delineation of the primary visual cortex (V1) (see Figs. 7 and 8). V1 is considered a hallmark of unique cortical lamination in the visual system, which has been previously delineated successfully through the use of high-resolution region-specific T1 MRI, focusing on the stripe of Gennari (Barbier et al. 2002; Geyer et al. 2011; Turner et al. 2008). In other words, despite the low resolution of our T1 data set, whole-brain surface projections of the layer probability maps demonstrate delineation or brain regions that have previously been delineated by high-resolution investigation.

It is important to note that when discussing our results, we use the term ‘T1 layer’, avoiding the traditional term ‘cortical layer’. The reasoning behind this phrasing is that T1 is not considered a direct measure of cytoarchitecture. Although multi-T1 methods investigate the laminar structure of the cortex, even high-resolution T1 MRI averages contributions of many cells, including but not limited to neurons and glial cells (Barbier et al. 2002; Barazany and Assaf 2012).

The main limiting factor of our method is the number of TIs chosen in the IR EPI sequence, which has significant impact on the probabilistic classification to T1 layers. Although our method is surface-based, it is less affected by the accuracy of cortical surface modeling, thanks to the spheres’ invariance to rotation. Nonetheless, the surface-based nature of our approach can still be considered a minor limiting factor. These limiting factors can easily be dealt with by increasing the number of TIs and thus potentially increasing the accuracy of T1 layer classification, or by

increasing the resolution of the anatomic MPRAGE image (from 1 mm to 600 µm, for example), thus increasing the accuracy of the cortical surfaces. Choice of these image acquisition parameters is an act of checks and balances, with acquisition time and image resolution on either sides of the scale.

The automatic whole-brain applicability of the method could enable future analysis of large populations. Such larger scale studies of groups of healthy subjects could provide a closer look at both the statistics of T1 layer characteristics, as well as regional layer transition effects, including compositional layer variability between the gyral wall and the cap of the gyri.

It has long been accepted that the laminar structure of the cortex plays an integral role in cognition, physiology, and different pathologies. For instance, certain forms of epilepsy have been linked to cortical dysplasia, a pathology involving abnormalities of the laminar structure of the cortex, which could be further studied using in-vivo subcortical imaging (Tassi et al. 2002). We suggest that the robust automatic tool presented here could potentially be used as a framework for quantitative expansion of such studies into the role of cortical thickness in brain function and behavior to the cortical layer level.

References

Annese J, Pitiot A, Dinov ID, Toga AW (2004) A myelo-architectonic method for the structural classification of cortical areas. NeuroImage 21:15–26. https://doi.org/10.1016/j.neuroimage.2003.08.024

Ballester MAG, Zisserman AP, Brady M (2002) Estimation of the partial volume effect in MRI. Med Image Anal 6:389–405. https://doi.org/10.1016/S1361-8415(02)00061-0

Barazany D, Assaf Y (2012) Visualization of cortical lamination patterns with magnetic resonance imaging. Cereb Cortex 22:2016–2023. https://doi.org/10.1093/cercor/bhr277

Barbier EL, Marrett S, Danek A, Vortmeyer A, van Gelderen P, Duyn J, Bandettini P, Grafman J, Koretsky AP (2002) Imaging cortical anatomy by high-resolution MR at 3.0T: detection of the stripe of gennari in visual area 17. Magn Reson Med 48:735–738. https://doi.org/10.1002/mrm.10255

Beul SF, Hilgetag CC (2014) Towards a "canonical" agranular cortical microcircuit. Front Neuroanat 8:165. https://doi.org/10.3389/fnana.2014.00165

Bridge H, Clare S (2006) High-resolution MRI: in vivo histology? Philos Trans R Soc 361:137–146. https://doi.org/10.1098/rstb.2005.1777

Clare S, Bridge H (2005) Methodological issues relating to in vivo cortical myelography using MRI. Hum Brain Mapp 26:240–250. https://doi.org/10.1002/hbm.20162

Clark VP, Courchesne E, Grafe M (1992) In vivo myeloarchitectonic analysis of human striate and extrastriate cortex using magnetic resonance imaging. Cereb Cortex 2:417–424. https://doi.org/10.1093/cercor/2.5.417

Deistung A, Schafer A, Schweser F, Biedermann U, Turner R, Reichenback JR (2013) Toward in vivo histology: a comparison of quantitative susceptibility mapping (QSM) with magnitude-, phase-, and R2*-imaging at ultra-high magnetic field strength. NeuroImage 65:299–314. https://doi.org/10.1016/j.neuroimage.2012.09.055

Dinse J, Hartwich N, Waehnert MD, Tardif CL, Schafer A, Geyer S, Preim B, Turner R, Bazin PL (2015) A cytoarchitecture-driven myelin model reveals area-specific signatures in human primary and secondary areas using ultra-high resolution in-vivo brain MRI. NeuroImage 114:71–87. https://doi.org/10.1016/j.neuroimage.2015.04.023

Duyn JH, van Gelderen P, Li TQ, de Zwart JA, Koretsky AP, Fukunaga M (2007) High-field MRI of brain cortical substructure based on signal phase. PNAS 104:28:11796–11801. https://doi.org/10.1073/pnas.0610821104

Fischl B (2012) FreeSurfer. NeuroImage 62:774–781. https://doi.org/10.1016/j.neuroimage.2012.01.021

Fischl B, Dale AM (2010) Measuring the thickness of the human cerebral cortex from magnetic resonance images. PNAS 97:20:11050–11055. https://doi.org/10.1073/pnas.200033797

Fischl B, van der Kouwe A, Destrieux C, Halgren E, Segonne F, Salat DH, Busa E, Seidman LJ, Goldstein J, Kennedy D, Caviness V, Makris N, Rosen B, Dale AM (2004) Automatically parcellating the human cerebral cortex. Cereb Cortex 14:11–22. https://doi.org/10.1093/cercor/bhg087

Fracasso A, van Veluw SJ, Visser F, Luijten PR, Spliet W, Zwanenburg JJM, Dumoulin SO, Petridou N (2016) Lines of Baillarger in vivo and ex vivo: Myelin contrast across lamina at 7T MRI and histology. NeuroImage 133:163–175. https://doi.org/10.1016/j.neuroimage.2016.02.072

Garey LJ (2006) Brodmann's localization in the cerebral cortex. Springer: Berlin 1–58. https://doi.org/10.1142/p151

Geyer S, Weiss M, Reimann K, Lohmann G, Turner R (2011) Microstructural parcellation of the human cerebral cortex—from brodmann's post-mortem map to in vivo mapping with high-field magnetic resonance imaging. Front Hum Neurosci. https://doi.org/10.3389/fnhum.2011.00019

Glasser MF, Goyal MS, Preuss TM, Raichle ME, Van Essen DC (2014) Trends and properties of human cerebral cortex: correlations with cortical myelin content. NeuroImage 93:165–175. https://doi.org/10.1016/j.neuroimage.2013.03.060

Kiernan J, Rajakumar N (2014) Barr's the human nervous system—an anatomical viewpoint. Lippincott Williams & Wilkins, Philadelphia, USA, pp 213–246

Lifshits S, Tomer O, Shamir I, Barazany D, Tsarfaty G, Rosset S, Assaf Y (2018) Resolution considerations in imaging of the cortical layers. NeuroImage 164:112–120. https://doi.org/10.1016/j.neuroimage.2017.02.086

Lutti A, Dick F, Sereno MI, Weiskopf N (2014) Using high-resolution quantitative mapping of R1 as an index of cortical myelination. NeuroImage 93:176–188. https://doi.org/10.1016/j.neuroimage.2013.06.005

MacDonald D, Kabani N, Avis D, Evans AC (2000) Automated 3-D extraction of inner and outer surfaces of cerebral cortex from MRI. NeuroImage 12:340–356. https://doi.org/10.1006/nimg.1999.0534

Peel D, McLachlan GJ (2000) Robust mixture modelling using the t distribution. Stat Comput 10(4):339–348. https://doi.org/10.1023/A:1008981510081

Scholtens LH, de Reus MA, van den Heuvel MP (2015) Linking contemporary high resolution magnetic resonance imaging to the von economo legacy: a study on the comparison of MRI cortical thickness and histological measurements of cortical structure. Hum Brain Mapp 36:3038–3046. https://doi.org/10.1002/hbm.22826

Scholtens LH, de Reus MA, de Lange SC, Schmidt R, van den Heuvel MP (2016) An MRI von economo—koskinas atlas. NeuroImage 170:249–256. https://doi.org/10.1016/j.neuroimage.2016.12.069

Shafee R, Buckner RL, Fischl B (2015) Gray matter myelination of 1555 human brains using partial volume corrected MRI images. NeuroImage 105:473–485. https://doi.org/10.1016/j.neuroimage.2014.10.054

Tassi L, Colombo N, Garbelli R, Francione S, Lo Russo G, Mai R, Cardinale F, Cossu M, Ferrario A, Galli C, Bramerio M, Citterio A, Spreafico R (2002) Focal cortical dysplasia: neuropathological subtypes, EEG, neuroimaging and surgical outcome. Brain 125:1719–1732. https://doi.org/10.1093/brain/awf175

Tomer O, Baratz Z, Shamir I, Kaptzon D, Horowitz A, Faraggi M, Barazany D, Assaf Y (2018) A probabilistic method for modelling cortical layer composition in sub-voxel resolution. Poster session presented at the Organization for Human Brain Mapping Association, Singapore. https://ww5.aievolution.com/hbm1801/index.cfm?do=ev.viewEv&ev=1317. Accessed 20 June 2018

Turner R, Oros-Peusquens AM, Romanzetti S, Zilles K, Shah NJ (2008) Optimised in vivo visualisation of cortical structures in the human brain at 3 T using IR-TSE. Magn Reson Imaging 26:935–942. https://doi.org/10.1016/j.mri.2008.01.043

Von Bonin G (1950) Essay on the cerebral cortex. Oxford: C. C. Thomas. https://doi.org/10.1001/jama.1950.02920110084053

Waehnert MD, Dinse J, Weiss M, Streicher MN, Waehnert P, Geyer S, Turner R, Bazin PL (2014) Anatomically motivated modeling of cortical laminae. NeuroImage 93:210–220. https://doi.org/10.1016/j.neuroimage.2013.03.078

Waehnert MD, Dinse J, Schafer A, Geyer S, Bazin PL, Turner R, Tardif CL (2016) A subject-specific framework for in vivo myeloarchitectonic analysis using high resolution quantitative MRI. NeuroImage 125:94–107. https://doi.org/10.1016/j.neuroimage.2015.10.001